CrystEngComm

PAPER

View Article Online
View Journal | View Issue

Cite this: *CrystEngComm*, 2014, **16**, 10780

Effect of high pressure on the crystal structure and charge transport properties of the (2-fluoro-3-pyridyl)(4-iodophenyl)borinic 8-oxyquinolinate complex†

Grzegorz Wesela-Bauman,*[ab] Simon Parsons,[c] Janusz Serwatowski[a] and Krzysztof Woźniak[b]

Received 22nd August 2014,
Accepted 1st October 2014

DOI: 10.1039/c4ce01730g

www.rsc.org/crystengcomm

The crystal and molecular structure of (2-fluoro-3-pyridyl)(4-iodophenyl)borinic 8-oxyquinolinate has been determined at room temperature at pressures ranging from ambient to 4.9 GPa in approximately 1 GPa steps. The crystal structure symmetry is conserved during the compression while the *a*, *b* and *c* unit cell dimensions were compressed by 7.5%, 8.0% and 6.9%, respectively. The crystal cell volume decreased by 19.4%. The analysis of the compression of the crystal was supported by computational results obtained with the PASCAL code. They proved that the crystal compression proceeds almost isotropically. A combination of Hirshfeld surface analysis and PIXEL calculations indicated the formation of multiple new contacts involving fluorine···fluorine and iodine···π-density. Energies of interactions calculated for the observed motifs present in the crystal were rationalized on the basis of contacts observed for these motifs. Further analysis based on the Marcus model was performed to trace the possible changes in the charge transport properties of the crystal. The analysis showed that electron and hole transport properties are not affected in the same way by the compression. However, hydrostatic pressure did not affect which charge transport (electron or hole) is the dominant one for this material.

Introduction

8-Oxyquinolinate complexes, MQ_n (n = 1, 2, 3) (M is a trivalent metal and Q is 8-oxyquinolinate), are widely used in organic light-emitting diodes (OLEDs) as light emitters and charge carriers.[1] Although materials with M = Al were frequently used both as emitting materials[2] and as charge transport carriers,[3] their good optical properties were counterbalanced by long-term instability leading to degradation of the diode.[4,5] Hence, analogues of aluminium were investigated, mainly GaQ_3 and InQ_3 complexes.[6–8] Finally, borinic complexes turned out to be more stable and more efficient emitters than aluminium[9,10] and became widely investigated.[11–15] For MQ_n (n = 1, 2, 3) complexes, it is commonly believed that the HOMOs span across the phenolate ring and the LUMOs across the pyridine ring of 8-oxyquinolinate. Those orbitals are involved in processes of electron excitation and relaxation followed by photon emission. The energies of the frontier orbitals can be affected by either chemical functionalisation (by attaching electron donating or withdrawing groups)[16–18] or modification of their crystal structure which was proven by high pressure studies on structures of AlQ_3, GaQ_3 and InQ_3.[19]

An important parameter of a particular material, from the standpoint of application in OLEDs, is the charge transfer character and its rate.[20,21] In this matter, it is interesting that some authors were able to point out the correlation between the degree of intermolecular π–π interactions and charge transport properties and electroluminescence.[22,23] However, in those papers the authors were simultaneously changing the molecular and, as a consequence, supramolecular structure. Studies of the influence of the crystal phase without affecting the molecular structure were done on AlQ_3.[24] A broader description of the impact of molecular arrangements was done with computational studies.[25–33] This approach assumes that carrier mobility (μ) in the hopping process is

[a] *Physical Chemistry Department, Faculty of Chemistry, Warsaw University of Technology, Noakowskiego 3, 00-664 Warszawa, Poland. E-mail: grzegorz.wesela@chem.uw.edu.pl*
[b] *Department of Chemistry, University of Warsaw, Pasteura 1, 02-093 Warszawa, Poland*
[c] *School of Chemistry and Centre for Science at Extreme Conditions, The University of Edinburgh, King's Buildings, West Mains Road, Edinburgh EH9 3JJ, Scotland, UK*

† Electronic supplementary information (ESI) available. CCDC 993575–993581. For ESI and crystallographic data in CIF or other electronic format see DOI: 10.1039/c4ce01730g

related to the charge transfer rate (k_{CT}) *via* the Einstein eqn (1):

$$\mu = \frac{ed^2}{k_B T} k_{CT} \quad (1)$$

where k_B is the Boltzmann constant, T is temperature, e the electronic charge, and d is the transport distance. The charge transport rate can be calculated using the Marcus–Hush theory.[34–36] The charge transport (CT) rate constant, k_{CT}, can be evaluated by the following eqn (2):

$$k_{CT} = \frac{2\pi}{\hbar} H_{AB}{}^2 \frac{1}{\sqrt{4\pi \Lambda k_B T}} \exp\left(-\frac{\left(\Delta G^o - \Lambda\right)^2}{4 \Lambda k_B T} \right) \quad (2)$$

where Λ is the reorganization energy, $H_{AB}{}^2$ is the transfer integral which represents the electronic coupling between donor and acceptor, T is the temperature, ΔG^o is the standard free enthalpy and k_B is the Boltzmann constant. Since we analyse hopping of charge carriers between molecules of the same compound than the standard free enthalpy is equal to zero ($\Delta G^o = 0$). Furthermore the reorganization energy (Λ) is a constant value for a particular compound. The only parameter affected by interactions in the crystal state is the transfer integral (H_{AB}). The greater the values of the transfer integral for a particular type of charge carriers (for a single contact) are, the better the pathway for charge hopping such contact is ($\mu \sim H_{AB}$). This integral is related to the energy splitting (ΔE) of the electronic level of two interacting molecules (Fig. 1).

H_{AB} for hole and electron transport is equal to half of the energy difference between HOMO and HOMO − 1 and LUMO and LUMO + 1 energy levels, respectively.

Recently, we have investigated the influence of functionalization on the photophysical properties of (2-fluoro-3-pyridyl)arylborinic 8-oxyquinolinates.[37] In this paper, we extend these investigations by determining the effect of pressure on the crystal structure of (2-fluoro-3-pyridyl)(4-iodophenyl)borinic 8-oxyquinolinate (**1**, Fig. 2) and its charge transfer properties.

In this contribution, the crystal structure of **1** at pressures ranging from ambient to 4.9 GPa is presented. The impact of high pressure on weak interactions is described and discussed. Experimental results are supported by theoretical analysis of the influence of pressure on the charge carrier properties in the framework of the Marcus theory.

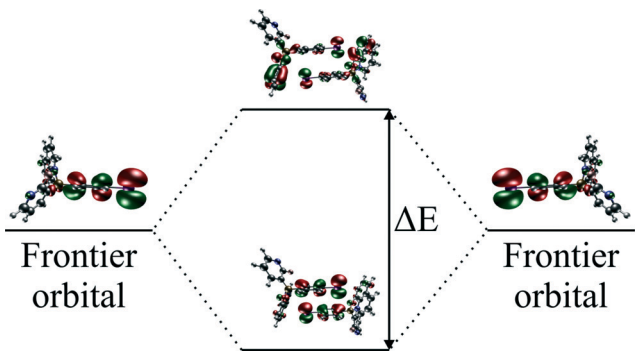

Fig. 1 Energy splitting of the frontier orbitals.

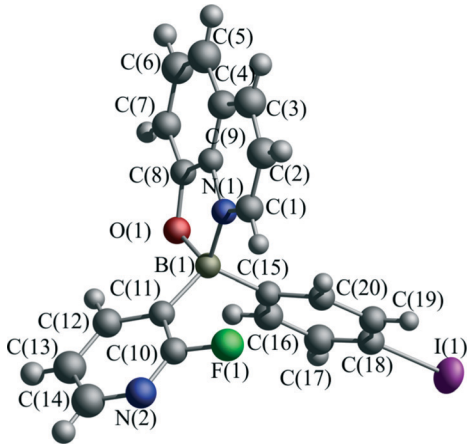

Fig. 2 Molecular structure and atom labelling scheme of complex **1**.

Experimental section

Synthesis, crystal growth and high-pressure crystallography

The title compound was synthesized according to our previous report.[37] Crystals of **1** were grown by slow evaporation of acetone from a concentrated solution of **1**. One block-shaped crystal of dimensions 0.2 mm × 0.2 mm × 0.25 mm was selected and loaded into a Merrill–Bassett diamond anvil cell (DAC).[38,39] The cell total opening angle was 80°, and the cell was equipped with 600 μm culets and a tungsten gasket. A 4 : 1 mixture of methanol and ethanol was used as a hydrostatic medium. A small piece of ruby was also put into the cell as the pressure marker by the ruby fluorescence method used to measure the pressure.[40]

Data collection, reduction and refinement

Single-crystal X-ray data collection was conducted at ambient pressure and at 0.17, 1.09, 2.04, 3.02, 3.96 and 4.88 GPa. All high-pressure data were collected at ambient temperature. Diffraction data were collected on a Bruker APEX II diffractometer with graphite-monochromated MoK_α radiation (λ = 0.71073 Å).[41] The data were integrated using SAINT[42] and an absorption correction was performed with the SADABS program.[43] Dynamic masking was applied during integration of the high-pressure data sets.[44]

The structure under ambient conditions was solved using the SUPERFLIP[45] program implemented in CRYSTALS.[46] The independent atom model (IAM) refinement based on F was performed with the CRYSTALS package. Optimised weighting schemes based on Chebychev polynomials were used for all refinements.[47] Atomic scattering factors in their analytical form were taken from the International Tables for Crystallography.[48] All non-hydrogen atoms (except iodine) were refined isotropically and all of the hydrogen atoms were

placed in idealized positions within the riding model for atomic displacement parameters (ADPs) (with $U_{iso}^{H} = 1.2 \cdot U_{eq}^{C}$) in order to retain a data-to-parameter ratio greater than 24. All hydrogen atoms were clearly visible on the difference density maps. Coordinates (and ADPs) of **1** were refined against these ambient pressure X-ray data to yield a conventional R_1 factor of 5.1% for 2650 data with $I > 2\sigma(I)$.

Each data set was restricted to 0.84 $Å^{-1}$ resolution in order to have a meaningful comparison of the geometries obtained from the experiments. For every collected dataset the $F_o^2 > 2\sigma(F_o^2)$ criterion, adopted from SHELX, was used only for calculating R factors and is not relevant to the choice of reflections for the refinement.

Starting models for the high-pressure structures were taken from the coordinates determined in the previous step. Minimization was performed against F using data with $I > 2\sigma(I)$. The completeness of the data sets ranged from 37% to 46%, and only the iodine was refined with anisotropic displacement parameters, all other atoms being modelled isotropically. It is worth mentioning that the data quality for all of the pressure steps was sufficient enough to perform anisotropic refinement of the ADPs for all of the atoms (not just for the iodine atom).

All hydrogen atoms were clearly visible on the difference density maps. Hydrogen atoms were placed in idealized positions and allowed to ride on their parent atoms with $U_{iso}^{H} = 1.2 \cdot U_{eq}^{C}$. All bond distances and angles were restrained to values observed in the ambient pressure structure. Details of data collection and refinement are provided in Table 1 and, with more details, in the ESI† (Table S1).

CCDC 993575–993581 contains the supplementary crystallographic data (CIF files) for crystals studied in this work.

Theoretical calculations and visualization

Energies of intermolecular interactions were calculated using the PIXEL method.[49–52] For comparison of results obtained with PIXEL and DFT and post-HF methods see ref. 53. All quantum calculations were carried out using the GAUSSIAN09 package.[54] Calculation of the frontier orbital energies employed the B3LYP[55,56] and B97D[57] DFT potentials combined with the 6-31+g(d,p)[58] basis set. The LANL2DZ[59] basis set with its complete core relativistic effective core potential was used for the iodine atom. Additional *d* and *f* functions were added to the LANL2DZ basis set according to the modification proposed by Glukhovtsev *et al.*[60] Benchmark calculations demonstrated that this modification improves obtained bond lengths and bond energies leading to more accurate results.[61,62] Our previous work implementing this modification showed good correlation between experimental and theoretically obtained UV-vis spectra.[37] Electron density was evaluated with the DGDZVP[63,64] basis set. C–H distances were

Table 1 Selected crystallographic data for compound **1**

Experimental details	(1) T = 296 K ambient	(2) T = 296 K P = 0.17 GPa	(3) T = 296 K P = 1.09 GPa	(4) T = 296 K P = 2.04 GPa	(5) T = 296 K P = 3.02 GPa	(6) T = 296 K P = 3.96 GPa	(7) T = 296 K P = 4.88 GPa
Chemical formula	$C_{20}H_{13}BFIN_2O$	$C_{20}H_{13}BFIN_2O$	$C_{20}H_{13}BFIN_2O$	$C_{20}H_{13}BFIN_2O$	$C_{20}H_{13}BFIN_2O$	$C_{20}H_{13}BFIN_2O$	$C_{20}H_{13}BFIN_2O$
M_r	454.03	454.03	454.03	454.03	454.03	454.03	454.03
Crystal system	Monoclinic	Monoclinic	Monoclinic	Monoclinic	Monoclinic	Monoclinic	Monoclinic
Space group	$P2_1/n$	$P2_1/n$	$P2_1/n$	$P2_1/n$	$P2_1/n$	$P2_1/n$	$P2_1/n$
Cell settings: a, b, c (Å)	6.8581(2)	6.8234(4)	6.6545(2)	6.5502(4)	6.4636(2)	6.4012(4)	6.3469(5)
	14.7849(4)	14.7074(7)	14.3261(5)	14.1051(7)	13.8775(5)	13.7152(9)	13.6039(10)
	17.3015(6)	17.200(2)	16.7183(14)	16.497(3)	16.3094(16)	16.187(3)	16.105(3)
α, β, γ (°)	90.000	90.000	90.000	90.000	90.000	90.000	90.000
	90.966(2)	90.814(7)	90.460(5)	90.396(8)	90.317(5)	90.438(8)	90.549(10)
	90.000	90.000	90.000	90.000	90.000	90.000	90.000
V ($Å^3$)	1754.06(9)	1725.9(2)	1593.75(15)	1524.1(3)	1462.91(16)	1421.1(3)	1390.5(3)
Z	4	4	4	4	4	4	4
d (Mg m^{-3})	1.719	1.747	1.892	1.979	2.061	2.122	2.169
Crystal form, colour	Block, green	Block, green	Block, green	Block, green	Block , green	Block , green	Block , green
Crystal size (mm)	0.20 × 0.20 × 0.25	0.20 × 0.20 × 0.25	0.20 × 0.20 × 0.25	0.20 × 0.20 × 0.25	0.20 × 0.20 × 0.25	0.20 × 0.20 × 0.25	0.20 × 0.20 × 0.25
No. of measured,	34 795	9268	8787	7648	8296	6840	6772
independent and observed	5362	1184	1141	1067	1138	1142	1187
$[F^2 > 2\sigma(F^2)]$	2650	936	887	871	949	916	910
Criterion for observed reflection	$I > 2.00\sigma(I)$	$I > 2.00\sigma(I)$	$I > 2.00\sigma(I)$	$I > 2.00\sigma(I)$	$I > 2.00\sigma(I)$	$I > 2.00\sigma(I)$	$I > 2.00\sigma(I)$
Completeness (%)	100	37	39	38	42	44	46
R_{int} (%)	6.5	5.6	4.3	4.0	4.3	4.4	5.7
Θ_{max}	30.53	25.38	25.38	25.38	25.33	25.35	25.54
Refinement on	F	F	F	F	F	F	F
R $[F^2 > 2\sigma(F^2)]$	0.0510	0.0501	0.0354	0.0326	0.0339	0.0340	0.0392
wR (F^2)	0.0512	0.0396	0.0385	0.0348	0.0355	0.0367	0.0417
GooF	1.000	1.000	1.000	1.000	1.000	1.000	1.000
No. of reflections	2650	936	887	871	949	916	910
No. of parameters	110	110	110	110	110	110	110
$\Delta\rho_{max}$, $\Delta\rho_{min}$ (e $Å^{-3}$)	0.70, −0.78	0.40, −0.40	0.58, −0.43	0.37, −0.30	0.46, −0.33	0.34, −0.50	0.52, −0.66

normalized prior to calculations to the standard neutron value of 1.083 Å.[65] Visualization of the crystal structures and frontier orbitals was achieved using the DIAMOND[66] and the VMD[67] programs, respectively. The electrostatic potential was calculated and visualized with AIMALL.[68] Hirshfeld surface analysis was performed with CRYSTALEXPLORER.[69–72]

Results and discussion

Molecular shape

The tetrahedral character of the coordination sphere of the boron atom is not affected by pressure. The bond lengths of the dative bonds: B–N, and B–O, and B–C are equal within

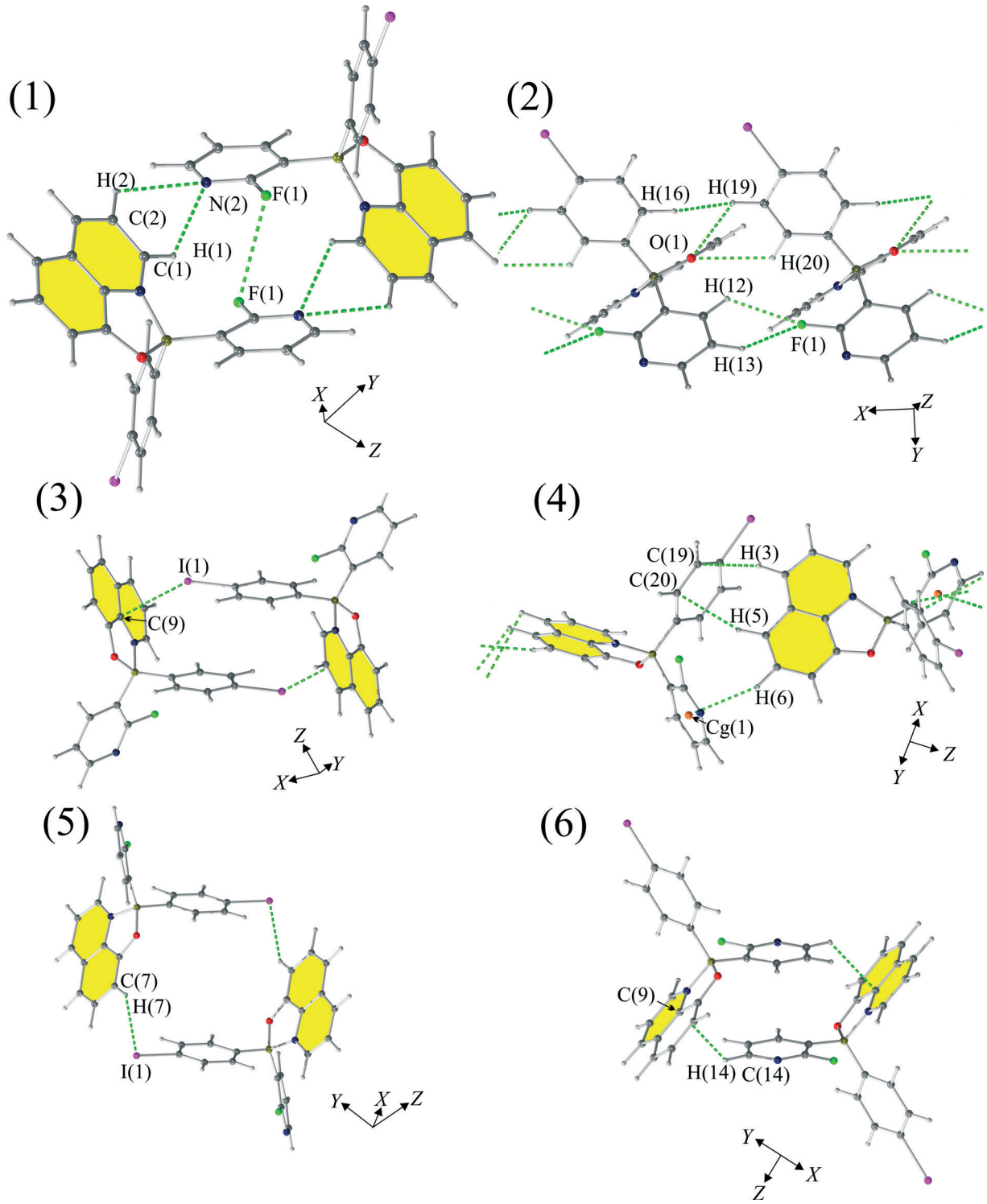

Fig. 3 Motifs (1)–(6) observed in the crystal structure of **1**.

the error at all pressures studied (Table S2†). Similarly, there are no significant differences in the molecular dimensions involving phenyl and pyridyl groups. High pressure slightly modifies the conformation of the molecule. The most pronounced differences between the ambient and the 4.9 GPa geometry of the moiety can be summarized as a twist of quinoline rings and deviation from planarity in the pyridine ring with interplanar angles of 3.6° and 5.7°, respectively (Fig. S6†). Hence, as expected for this material, the only thing that was affected by the pressure was the intermolecular interactions which can be directly related to the change in the CT properties.

The structure of 1 at ambient temperature and pressure

The supramolecular architecture of **1** is based on crystallographic motifs compromising weak interactions (Fig. 3 and 5). The strongest motif [see (1)] involves bifurcated hydrogen bond C(1)–H(1)···N(2) ($d_{H\cdots N}$ = 2.63 Å) and C(2)–H(2)···N(2) ($d_{H\cdots N}$ = 2.88 Å). The motif has an energy of −53.1 kJ mol^{-1} and a significant electrostatic (Fig. 3, Table 2) character. The impact of F(1)···F(1) interaction on the stability of this motif is not clear as the halogen–halogen distance is equal to $d_{F\cdots F}$ = 3.197(4) Å, which is relatively close to the sum of the van der Waals radii (2.94 Å).[73]

The second most energetic (2) motif comprises a bifurcated hydrogen bond: C(19)–H(19)···O(1) ($d_{H\cdots O}$ = 2.54 Å) and C(20)–H(20)···O(1) ($d_{H\cdots O}$ = 2.76 Å), with the energy of interactions equal to −40.7 kJ mol^{-1}. This is a dispersion-dominated motif which features interaction between 8-quinolinates. Repulsion, on the other hand, cannot be as easily rationalized by structural interactions as the mutual proximity of hydrogen–fluorine atoms, mainly C(12)–H(12)···F(1) and C(13)–H(13)···F(1) interactions (with interatomic distances equal to 2.67 Å and 2.81 Å, respectively) has larger distances than the distances observed in similar structures (2.43–2.73 Å).[37] For this motif we observed a mutual proximity of H(16) and H(19) atoms, but the distance between those hydrogens ($d_{H\cdots H}$ = 2.23 Å) is much greater than the approximate limit (1.7 Å) for such contacts established by Wood *et al.*[74]

The energy of interaction (3) in this case is dominated by repulsive interactions (101.5 kJ mol^{-1}), which is balanced by electrostatic (−48.8 kJ mol^{-1}) and dispersion terms (−67.1 kJ mol^{-1}). Those stabilizing contributions to the energy of (3) can be rationalized by the existence of a short intermolecular contact between C(9) and I(1) measuring 3.591(4) Å, and the interplanar contact between the 4-iodophenyl moieties with an interplanar distance of 4.024 Å.

The charge distribution of halogen moieties is not isotropic (Fig. 4), and the short distance is indicative of an interaction involving the σ-hole of the iodine and the π-electrons of the 8-oxyquinolinate rings. The repulsion between the π-electrons of 4-iodophenyl moieties and the negatively charged part of the iodine atom may be counterbalancing the attractive force between σ-hole and 8-oxyquinolinate rings.

The fourth motif (4) builds chains of molecules disposed about the 2_1 screw axis. Stabilization of this motif results from joint effects of dispersion (−38.3 kJ mol^{-1}) and the electrostatic interactions (−26.4 kJ mol^{-1}). This is achieved with a significant contribution of the C–H···π type interactions, mainly, C(6)–H(6)···Cg(1) ($d_{H\cdots Cg}$ = 2.88 Å, C(6)–H(6)–Cg(1) = 152), where Cg(1) is the centroid calculated for the 2-fluoro-3-pyridyl moiety. The largest contribution to the energy of interactions for this motif, according to the PIXEL calculations, is, as in the third motif, dominated by the repulsion term (42.4 kJ mol^{-1}).

Table 2 The comparison of the energies of interactions in the crystal structure of **1** at ambient pressure and at 4.9 GPa (italic) calculated using PIXEL

		Energy (kJ mol^{-1})					
	d (Å)[a]	Electrostatic	Polarization	Dispersion	Repulsion	Total	Symmetry
(1)	8.074	−42.7	−13.7	−24.9	28.2	−53.1	1 − *x*, 1 − *y*, 1 − *z*
	7.662	*−85.6*	*−29.6*	*−40.9*	*106.5*	*−49.6*	*1 − x, 2 − y, 1 − z*
(2)	6.858	−26.2	−11.1	−44.5	41.0	−40.7	*x* ± 1, *y*, *z*
	6.347	*−107.4*	*−45.6*	*−90.8*	*201.1*	*−42.8*	*x ± 1, y, z*
(3)	8.998	−48.8	−20.6	−67.1	101.5	−35.0	1 − *x*, −*y*, 1 − *z*
	8.406	*−193.0*	*−73.2*	*−128.7*	*363.0*	*−31.2*	*1 − x, 1 − y, 1 − z*
(4)	9.267	−26.4	−10.2	−38.3	42.4	−32.6	*x* ± 0.5, 0.5 − *y*, *z* ± 0.5
	8.638	*−98.6*	*−46.4*	*−80.9*	*197.5*	*−28.3*	*x ± 0.5, 1.5 − y, z ± 0.5*
(5)	8.485	−18.1	−6.7	−25.4	21.8	−28.4	−*x*, −*y*, 1 − *z*
	7.755	*−49.0*	*−26.1*	*−49.9*	*87.6*	*−37.3*	*−x, 1 − y, 1 − z*
(6)	7.498	−18.9	−10.9	−47.7	50.9	−26.6	−*x*, 1 − *y*, 1 − *z*
	6.942	*−95.8*	*−52.9*	*−94.2*	*224.8*	*−18.1*	*−x, 2 − y, 1 − z*
(7)	9.374	−1.9	−3.1	−13.8	5.4	−13.3	*x* ± 0.5, 0.5 − *y*, *z* ± 0.5
	8.695	*−21.2*	*−18.7*	*−37.1*	*53.6*	*−23.4*	*x ± 0.5, 1.5 − y, z ± 0.5*
(8)	12.336	−7.7	−2.7	−11.2	12.4	−9.2	0.5 − *x*, *y* ± 0.5, 1.5 − *z*
	11.738	*−25.4*	*−9.5*	*−21.7*	*45.7*	*−10.9*	*0.5 − x, y ± 0.5, 1.5 − z*
(9)	10.516	−2.7	−0.5	−1.9	0.0	−5.0	0.5 − *x*, *y* ± 0.5, 0.5 − *z*
	9.498	*−4.5*	*−0.8*	*−3.7*	*0.1*	*−8.8*	*0.5 − x, y ± 0.5, 0.5 − z*
(10)	12.970	−3.3	−0.1	−0.3	0.0	−3.6	2 − *x*, 1 − *y*, 1 − *z*
	12.718	*−2.8*	*−0.5*	*−4.5*	*0.6*	*−7.2*	*2 − x, 1 − y, 1 − z*

[a] Parameter *d* designates the distance between the centre of masses of two interacting molecules.

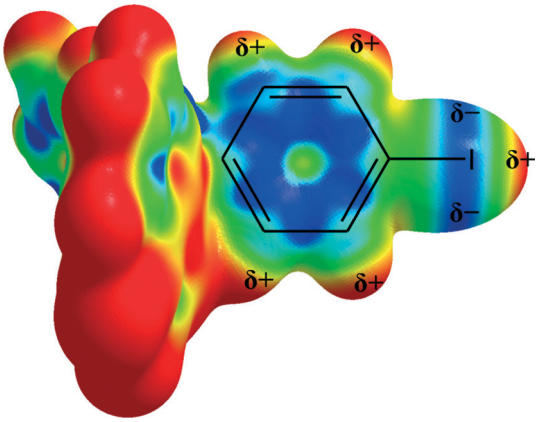

Fig. 4 Anisotropic charge distribution around the iodine atom in **1**. Electrostatic potential calculated at the B3LYP/DGDZVP level of theory.

The fifth motif (5) is also based on the anisotropy of the charge distribution of the iodine atom. It is stabilized by C(7)–H(7)···I(1) interactions in which a positively charged proton is pointing towards the negatively charged side of the iodine atom.

The sixth motif (6) is based upon two sets of interactions. The first set of interactions is based on C–H···π interactions, with the distance between C(9) and H(14) atoms from 2-fluoro-3-pyridyl moiety equaling to 2.86 Å. The other set of interactions is constructed from the π···π stacking interactions between 2-fluoro-3-pyridyl moieties with the interplanar distance equal to 3.780 Å. We believe that this interaction is strong, according to the calculations done by Sherrill *et al.*,[75] as such a distance is quite favourable for π···π interactions.

Motifs (7)–(10) (Fig. 5) compromise very weak interactions and are stabilized by either dispersion (motifs 7 and 8) and/or electrostatic contributions (motifs 8, 9 and 10). The seventh motif (7) has a short H(3)···H(16) contact (2.58 Å) and molecules in this motif are arranged in such a way that they create a chain of molecules. Similar chains are created by motifs (8) and (9 and stabilized by Q···Q interactions. Motif (10) compromises interacting molecules for which the mutual distance permits only electrostatic interactions.

Impact of pressure on the crystal structure of compound 1

Effect of pressure on the unit cell dimensions. Compound **1** is stable up to at least 4.9 GPa. The *a*, *b* and *c* unit cell dimensions decrease by 7.5%, 8.0%, and 6.9%, respectively. The *β* angle decreases by 0.4°. The volume of **1** is reduced by 19.4%. The lattice parameters as a function of pressure are shown in Fig. S1 and S2.† The degree of lattice distortion (DLD), calculated by the program STRAIN,[76–78] is equal to 0.0415 (for the output of the STRAIN program, see the ESI†).

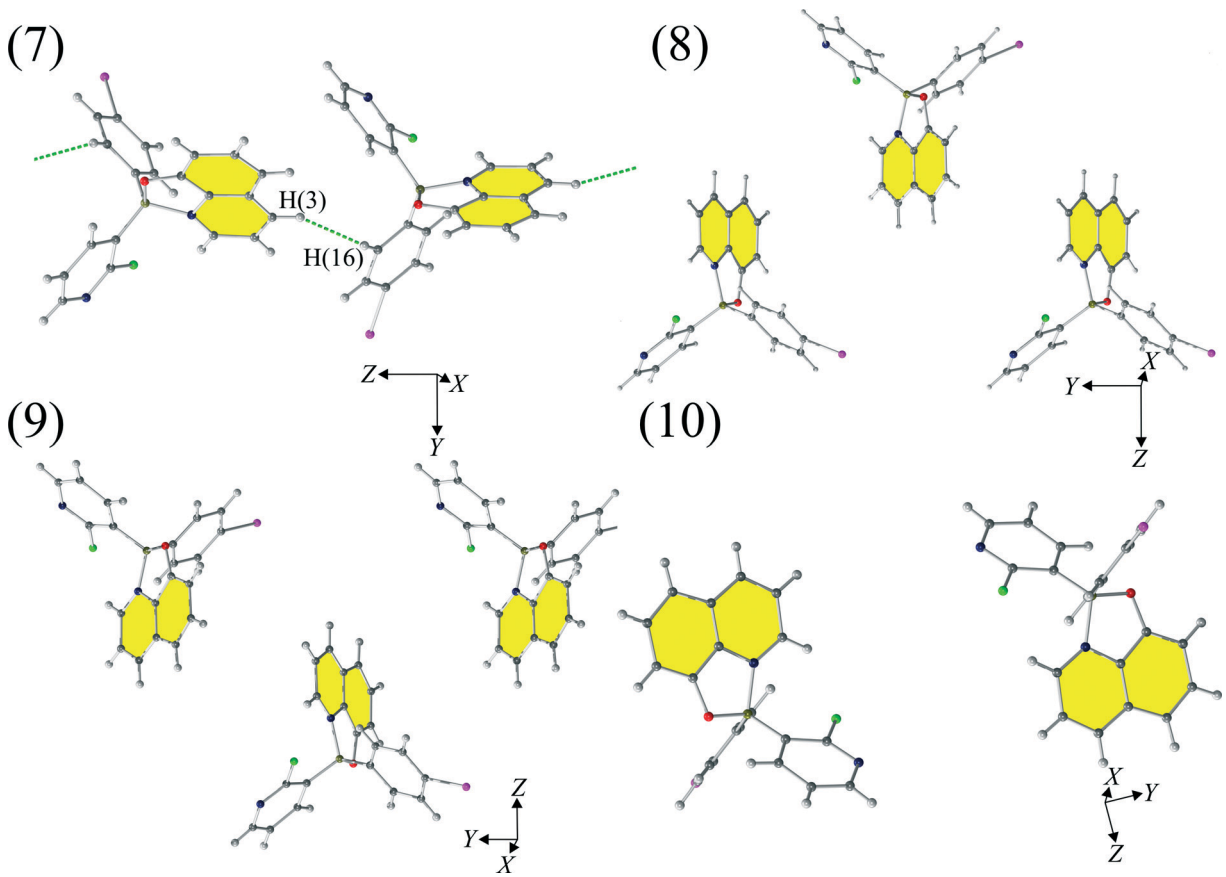

Fig. 5 Motifs (7)–(10) observed in the crystal structure of **1**.

For comparison, similar values of DLD can be obtained for ruthenium complexes at 4.63 GPa (0.0419),[79] and much lower values of DLD are observed for L-alanine at 4.31 GPa (0.0337).[80]

The changes in the variable-pressure parameters of the unit cell for this low-symmetry system are not strictly related to compressibility, which was presented by Cliffe *et al.*[81] Hence, we have implemented the PASCAL code for these calculations (for the output of the PASCAL program, see the ESI†).[81] Since the β angle is close to 90°, the PASCAL analysis gave similar results to the analysis for nonorthogonal a, b and c cell parameters. The direction of the greatest strain is close to the X axis (see orthonormalization matrix in the ESI†) and can be rationalized as a consequence of the lack of interactions parallel to that direction.

Analysis based on Birch–Murnaghan coefficients (B and B') may indicate a rapid stiffening of the described material ($B' > 4$) with pressure (for more details and comparison with other materials see the ESI†).

Effect of pressure on contact lengths and energies. The impact of pressure on the intermolecular contacts was

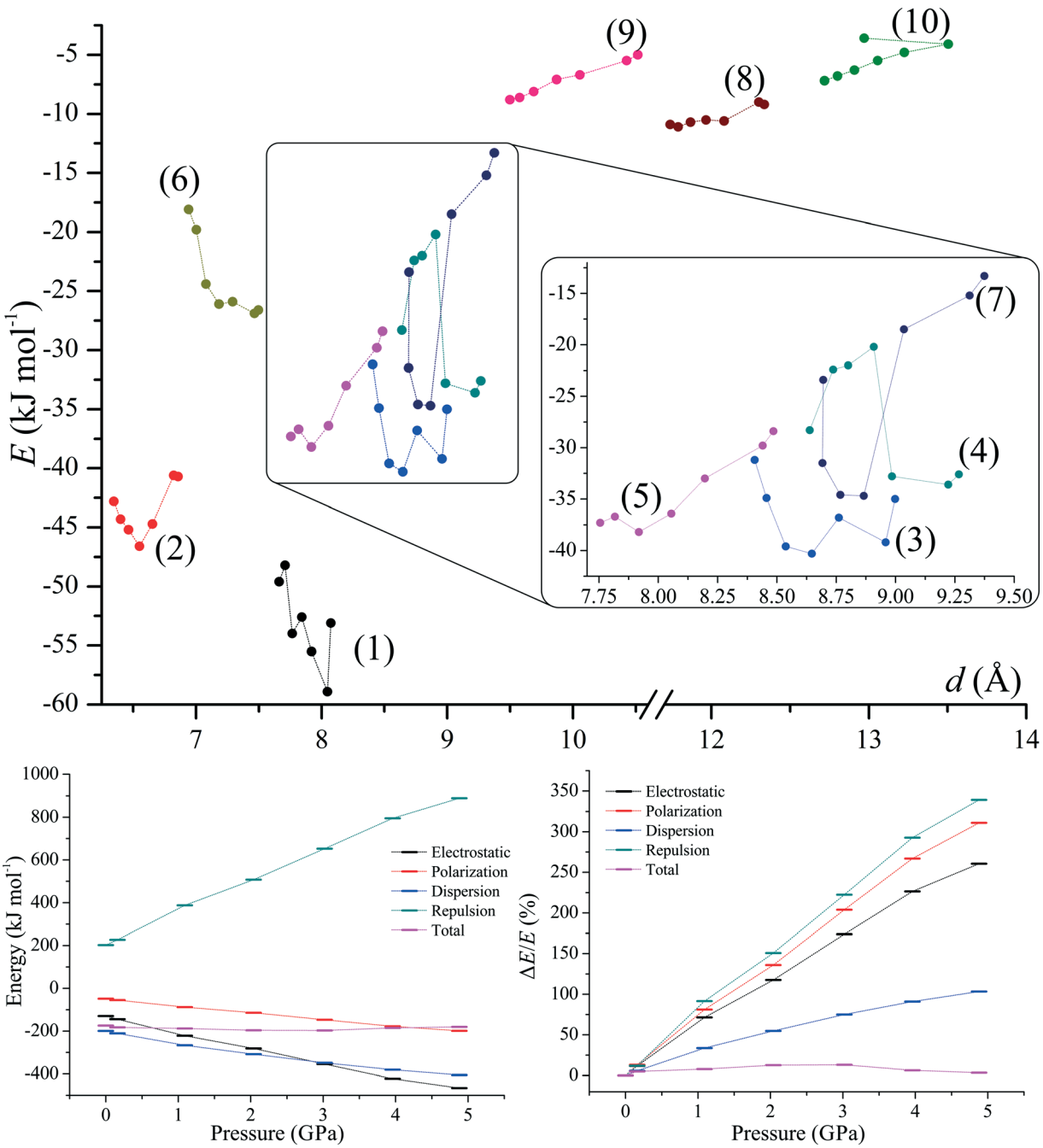

Fig. 6 Energies of motifs (1)–(10) as a function of distance (upper graph) and lattice energy (together with contributions from electrostatic, polarization, dispersion and repulsion) as a function of pressure (lower graphs) calculated using PIXEL.

evaluated through PIXEL calculations and is depicted in Fig. 6 (Fig. S9, Table S4–S10†). The increase in hydrostatic pressure results in shortening of intermolecular distances for all motifs. For motif (7) it seems that the change in pressure from 3.96 to 4.88 GPa did not affect the *d* parameter significantly. After initial compression, the distances of interactions for all motifs were lowered, but at higher pressures the effect of pressure was different depending on the nature of contacts present in the structure. The energies of motifs (2), (3), (5) and (7) during compression passed through a global energy minimum and then increased. On the other hand, motif (4) passed through the global maximum and then reached a local minimum at 4.9 GPa. The weakest motifs (*e.g.* (8), (9) and (10)) became more stable at each pressure step.

The effect of high pressure on the intermolecular interaction can be visualised using Hirshfeld (d_{norm}) surface analysis (Fig. S2–S4†). Red areas on the surface which represent contacts existing at ambient pressure become more pronounced after compression. New contacts appeared, especially H···H and C···H, but also F···F and N···H type contacts. Interactions between the iodine atom with both phenyl and Q rings become prominent at elevated pressure.

Compression has affected both lattice energies and contributions to the lattice energies (Fig. 6, lower graphs). As the compression progresses the total lattice energies decrease to reach a minimum at *ca.* 2.5 GPa and then their values start to increase. It seems that such behaviour is a consequence of the interplay between the polarization and the repulsion terms, which become more prominent with pressure (more than 3× stronger than those at ambient pressure, Tables S2–S3†).

Estimated change in the CT properties of 1 with pressure. Motifs described earlier were analyzed in terms of their charge transport properties using the Marcus theory. An interesting phenomenon is that a slight squeeze of the crystal improved electron transporting properties (understood as an increase of $H_{AB}(e^-)$) of the crystal and decreased the hole transporting properties (understood as a decrease of $H_{AB}(h^+)$) (Fig. 7). This is something that made the properties of the crystal more pronounced. It may also point to the fact that the pattern of interactions at this pressure is suppressing the hole transport. Further increase in the hydrostatic pressure resulted in a simultaneous increase of the $H_{AB}(e^-)$ and $H_{AB}(h^+)$; the former seem to be more affected by pressure.

It seems that crystallographic motifs are not participating in the CT properties equally, or that their character is not fixed during compression (Fig. 8a and b). The biggest contributions to the CT are from motifs (3), (4) and (7). Motif (3) with iodine···π-density interaction is almost solely a hole transporting contact whose CT properties are being increased with compression. It seems that this motif is being destabilized by pressure. On the other hand, motifs (4) and (7) have both dominating electron transporting properties. They also present the same pattern of CH···π interactions between Q and 2-fluoro-3-pyridyl and 4-iodophenyl rings. It

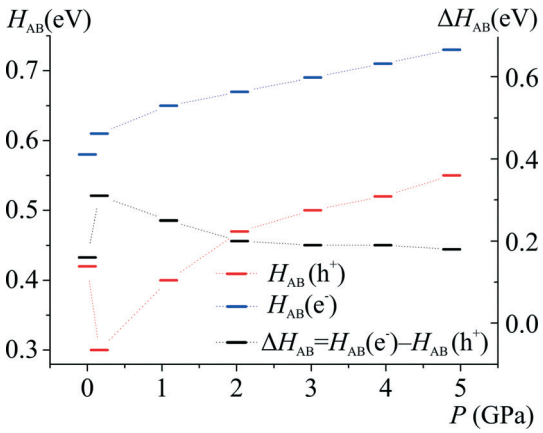

Fig. 7 Sum of charge transfer integrals as a function of hydrostatic pressure calculated at the B97D/6-31+g(d,p) level of theory.

seems that the mutual proximity between electron-rich phenolate ring and electron-deficient 2-fluoro-3-pyridyl ring favours transport of electrons. As the compression proceeds for (4) the electron CT properties are being hampered by increasing interactions between two electron-deficient rings, mainly pyridine and 2-fluoro-3-pyridyl. At 4.9 GPa the mutual orientation of molecules is similar to the orientation observed for normal pressure. Therefore, reinforcement of electron CT properties is observed. A similar situation is observed for motif (7). For pressure steps with close proximity of the phenolate ring and 2-fluoro-pyridyl the electron transporting properties were reinforced, whereas for the pressure steps which favour pyridine and 2-fluoro-pyridyl the CT properties were hampered. Observed trends in CT properties seem to be correlated with the stabilization energies (Fig. 6). For those two motifs, the stronger they are, the better CT properties they are presenting.

At this point it should be stressed that the PIXEL method was checked against various methods (DFT, post-HF).[53] The correlation was established against stabilization energies derived with PIXEL and *ab initio* methods leading to a conclusion that the method worked fine. However, in this contribution we are seeing that orbital overlapping (important from the standpoint of charge hopping) obtained with *ab initio* methods in some cases is correlated with motif energies obtained with PIXEL.

Apart from (3), motifs (2) and (5) also have their hole transporting properties dominating over electrons. This is due to the proximity of 4-iodophenyl rings which are occupied by HOMO orbitals. The CT character of motifs (8) and (9) was changed by the compression. It seems that the mutual orientation of molecules in those two motifs promotes better charge hopping than that present in motif (1).

Conclusions

The crystal of 1 was compressed almost isotropically which was confirmed by the analysis of the crystal lattice parameters supporting the analysis using PASCAL and STRAIN

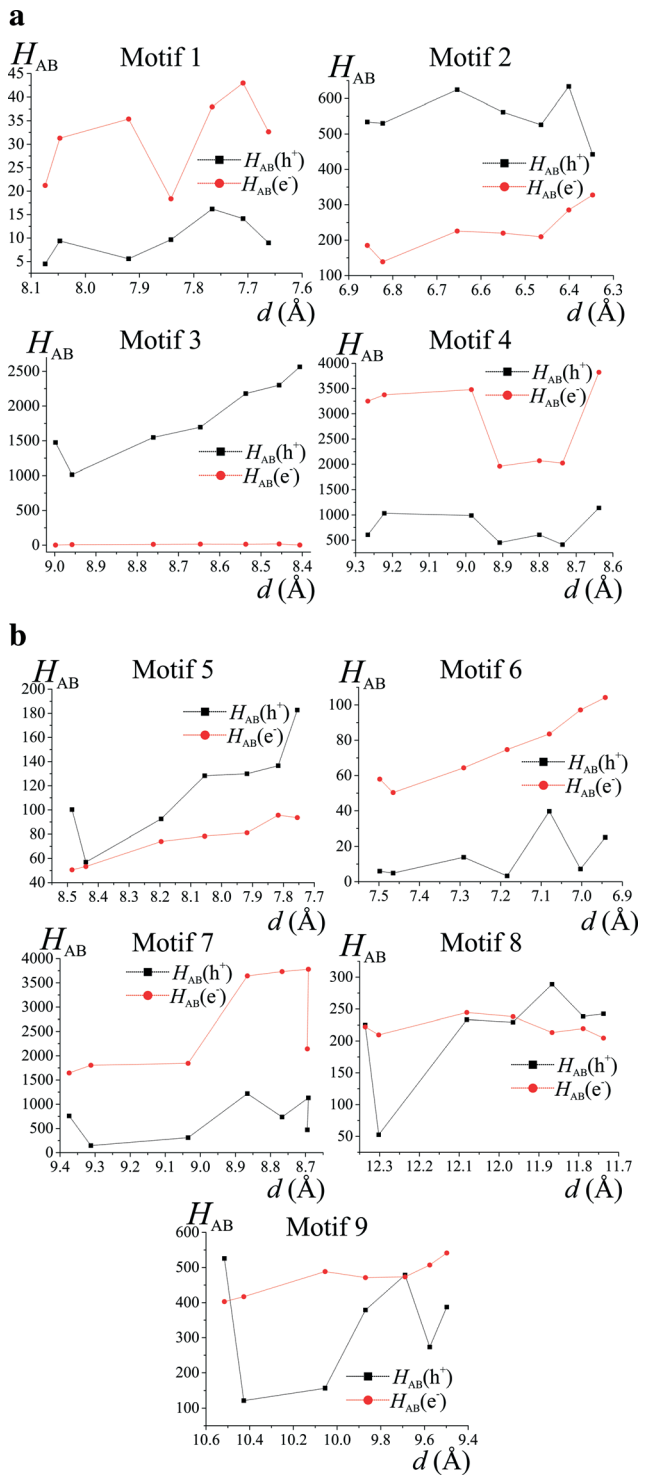

Fig. 8 a) Charge transfer integrals ($H_{AB}(10^{-4}$ eV)) for motifs (1)–(4) as a function of hydrostatic pressure calculated at the B97D/6-31+g(d,p) level of theory. b) Charge transfer integrals ($H_{AB}(10^{-4}$ eV)) for motifs (5)–(9) as a function of hydrostatic pressure calculated at the B97D/6-31+g(d,p) level of theory.

programs. While the molecular geometry remains virtually unchanged, the intermolecular interactions were affected greatly by the pressure. This was revealed qualitatively by Hirshfeld surface analysis and quantitatively by PIXEL calculations. Having a detailed description of a crystal system and changes triggered by the pressure, we could estimate how the structure affects the charge transport properties. It turns out that an increase in pressure improved charge transport properties estimated by the Marcus theory. It seems that motifs based on interactions between electron-rich and electron-poor ligands have strong electron transporting properties. On the other hand, interactions between two electron-deficient counterparts may hamper electron transporting properties.

Acknowledgements

The MPD/2010/4 project is realized within the MPD programme of the Foundation for Polish Science, cofinanced by the European Regional Development Fund. This work was supported by Warsaw University of Technology and by the Polish Ministry of Science and Higher Education (grant no. DEC-2011/03/B/ST5/02755). The support by Aldrich Chemical Co., Milwaukee, WI, USA, through continuous donation of chemicals and equipment is gratefully acknowledged. G.W.B. thanks the Foundation for Polish Science for financial support within the International PhD Program. Authors gratefully acknowledge the Interdisciplinary Centre for Mathematical and Computational Modelling in Warsaw (grant no. G33-14) for providing computer facilities on which most of the calculations were done. G.W.B. would like to thank Dr. Stephen Moggach, Mr. Andrew Maloney and Mr. Chris Cameron from the Chemical Crystallography Research Group at The University of Edinburgh.

References

1 C. H. Chen and J. Shi, *Coord. Chem. Rev.*, 1998, **171**, 161–174.
2 S. A. VanSlyke and C. W. Tang, *Appl. Phys. Lett.*, 1987, **51**, 913–915.
3 B. C. Lin, C. P. Cheng, Z.-Q. You and C.-P. Hsu, *J. Am. Chem. Soc.*, 2005, **127**, 66–67.
4 Z. D. Popovic, H. Aziz, A. Ioannidis, N.-X. Hu and P. N. M. dos Anjos, *Synth. Met.*, 2001, **123**, 179–181.
5 J. E. Knox, M. D. Halls, H. P. Hratchian and H. Bernhard Schlegel, *Phys. Chem. Chem. Phys.*, 2006, **8**, 1371–1377.
6 P. E. Burrows, L. S. Sapochak, D. M. McCarty, S. R. Forrest and M. E. Thompson, *Appl. Phys. Lett.*, 1994, **64**, 2718–2720.
7 P. Shakya, P. Desai, M. Somerton, G. Gannaway, T. Kreouzis and W. P. Gillin, *J. Appl. Phys.*, 2008, 103.
8 V. K. Shukla and S. Kumar, *Opt. Mater.*, 2007, **29**, 1809–1816.
9 S. Anderson, M. S. Weaver and A. J. Hudson, *Synth. Met.*, 2000, **111–112**, 459–463.
10 X.-Y. Wang and M. Weck, *Macromolecules*, 2005, **38**, 7219–7224.
11 K. Tanaka and Y. Chujo, *Macromol. Rapid Commun.*, 2012, **33**, 1235–1255.
12 F. Jäkle, *Chem. Rev.*, 2010, **110**, 3985–4022.
13 Y.-L. Rao and S. Wang, *Inorg. Chem.*, 2011, **50**, 12263–12274.

14 A. Nagai and Y. Chujo, *Chem. Lett.*, 2010, **39**, 430–435.
15 F. Jäkle, *Coord. Chem. Rev.*, 2006, **250**, 1107–1121.
16 Y. Qin, I. Kiburu, S. Shah and F. Jäkle, *Org. Lett.*, 2006, **8**, 5227–5230.
17 Y. Nagata and Y. Chujo, *Macromolecules*, 2008, **41**, 2809–2813.
18 Y. Tokoro, A. Nagai, K. Kokado and Y. Chujo, *Macromolecules*, 2009, **42**, 2988–2993.
19 I. Hernández and W. P. Gillin, *J. Phys. Chem. B*, 2009, **113**, 14079–14086.
20 U. Mitschke and P. Bauerle, *J. Mater. Chem.*, 2000, **10**, 1471–1507.
21 Y. Shirota and H. Kageyama, *Chem. Rev.*, 2007, **107**, 953–1010.
22 S. L. Hellstrom, J. Ugolotti, G. J. P. Britovsek, T. S. Jones and A. J. P. White, *New J. Chem.*, 2008, **32**, 1379–1387.
23 L. S. Sapochak, A. Padmaperuma, N. Washton, F. Endrino, G. T. Schmett, J. Marshall, D. Fogarty, P. E. Burrows and S. R. Forrest, *J. Am. Chem. Soc.*, 2001, **123**, 6300–6307.
24 M. Brinkmann, G. Gadret, M. Muccini, C. Taliani, N. Masciocchi and A. Sironi, *J. Am. Chem. Soc.*, 2000, **122**, 5147–5157.
25 Y.-K. Lan and C.-I. Huang, *J. Phys. Chem. B*, 2008, **112**, 14857–14862.
26 J.-L. Brédas, D. Beljonne, V. Coropceanu and J. Cornil, *Chem. Rev.*, 2004, **104**, 4971–5004.
27 G. R. Hutchison, M. A. Ratner and T. J. Marks, *J. Am. Chem. Soc.*, 2005, **127**, 16866–16881.
28 W.-Q. Deng and W. A. Goddard, *J. Phys. Chem. B*, 2004, **108**, 8614–8621.
29 V. Stehr, R. F. Fink, B. Engels, J. Pflaum and C. Deibel, *J. Chem. Theory Comput.*, 2014, **10**, 1242–1255.
30 M. Mamada, H. Katagiri, M. Mizukami, K. Honda, T. Minamiki, R. Teraoka, T. Uemura and S. Tokito, *ACS Appl. Mater. Interfaces*, 2013, **5**, 9670–9677.
31 H. Mori, X. Chen, N. Chang, S. Hamao, Y. Kubozono, K. Nakajima and Y. Nishihara, *J. Org. Chem.*, 2014, **79**, 4973–4983.
32 B. C. Lin, C. P. Cheng, Z.-Q. You and C.-P. Hsu, *J. Am. Chem. Soc.*, 2005, **127**, 66–67.
33 C. Liang and M. D. Newton, *J. Phys. Chem.*, 1992, **96**, 2855–2866.
34 R. A. Marcus and N. Sutin, *Biochim. Biophys. Acta, Rev. Bioenerg.*, 1985, **811**, 265–322.
35 P. F. Barbara, T. J. Meyer and M. A. Ratner, *J. Phys. Chem.*, 1996, **100**, 13148–13168.
36 E. Laborda, M. C. Henstridge, C. Batchelor-McAuley and R. G. Compton, *Chem. Soc. Rev.*, 2013, **42**, 4894–4905.
37 G. Wesela-Bauman, P. Ciećwierz, K. Durka, S. Luliński, J. Serwatowski and K. Woźniak, *Inorg. Chem.*, 2013, **52**, 10846–10859.
38 L. Merrill and W. A. Bassett, *Rev. Sci. Instrum.*, 1974, **45**, 290–294.
39 S. A. Moggach, D. R. Allan, S. Parsons and J. E. Warren, *J. Appl. Crystallogr.*, 2008, **41**, 249–251.
40 G. J. Piermarini, S. Block, J. D. Barnett and R. A. Forman, *J. Appl. Phys.*, 1975, **46**, 2774–2780.
41 Bruker AXS Inc., *SMART*, Bruker-Nonius, Madison, Wisconsin, USA, 2002.
42 Bruker AXS Inc., *SAINT*, Bruker-Nonius, Madison, Wisconsin, USA, 2004.
43 Bruker AXS Inc., *SADABS*, Madison, Wisconsin, USA, 2004.
44 A. Dawson, D. R. Allan, S. Parsons and M. Ruf, *J. Appl. Crystallogr.*, 2004, **37**, 410–416.
45 L. Palatinus and G. Chapuis, *J. Appl. Crystallogr.*, 2007, **40**, 786–790.
46 P. W. Betteridge, J. R. Carruthers, R. I. Cooper, K. Prout and D. J. Watkin, *J. Appl. Crystallogr.*, 2003, **36**, 1487.
47 J. R. Carruthers and D. J. Watkin, *Acta Crystallogr., Sect. A: Cryst. Phys., Diffr., Theor. Gen. Crystallogr.*, 1979, **35**, 698–699.
48 *International Tables for Crystallography: Mathematical, Physical and Chemical Tables*, ed. H. Fuess, Chester, 2006, vol. C.
49 A. Gavezzotti, *J. Phys. Chem. B*, 2003, **107**, 2344–2353.
50 A. Gavezzotti, *J. Phys. Chem. B*, 2002, **106**, 4145–4154.
51 A. Gavezzotti, *J. Chem. Theory Comput.*, 2005, **1**, 834–840.
52 A. Gavezzotti, *CrystEngComm*, 2003, **5**, 429–438.
53 L. Maschio, B. Civalleri, P. Ugliengo and A. Gavezzotti, *J. Phys. Chem. A*, 2011, **115**, 11179–11186.
54 M. J. Frisch, G. W. Trucks, H. B. Schlegel, G. E. Scuseria, M. A. Robb, J. R. Cheeseman, G. Scalmani, V. Barone, B. Mennucci, G. A. Petersson, H. Nakatsuji, M. Caricato, X. Li, H. P. Hratchian, A. F. Izmaylov, J. Bloino, G. Zheng, J. L. Sonnenberg, M. Hada, M. Ehara, K. Toyota, R. Fukuda, J. Hasegawa, M. Ishida, T. Nakajima, Y. Honda, O. Kitao, H. Nakai, T. Vreven, J. A. Montgomery Jr., J. E. Peralta, F. Ogliaro, M. Bearpark, J. J. Heyd, E. Brothers, K. N. Kudin, V. N. Staroverov, T. Keith, R. Kobayashi, J. Normand, K. Raghavachari, A. Rendell, J. C. Burant, S. S. Iyengar, J. Tomasi, M. Cossi, N. Rega, J. M. Millam, M. Klene, J. E. Knox, J. B. Cross, V. Bakken, C. Adamo, J. Jaramillo, R. Gomperts, R. E. Stratmann, O. Yazyev, A. J. Austin, R. Cammi, C. Pomelli, J. W. Ochterski, R. L. Martin, K. Morokuma, V. G. Zakrzewski, G. A. Voth, P. Salvador, J. J. Dannenberg, S. Dapprich, A. D. Daniels, O. Farkas, J. B. Foresman, J. V. Ortiz, J. Cioslowski and D. J. Fox, *Gaussian 09*, Gaussian, Inc, Wallingford CT, 2010.
55 A. D. Becke, *Phys. Rev. A: At., Mol., Opt. Phys.*, 1988, **38**, 3098–3100.
56 C. Lee, W. Yang and R. G. Parr, *Phys. Rev. B: Condens. Matter Mater. Phys.*, 1988, **37**, 785–789.
57 S. Grimme, *J. Comput. Chem.*, 2006, **27**, 1787–1799.
58 R. Krishnan, J. S. Binkley, R. Seeger and J. A. Pople, *J. Chem. Phys.*, 1980, **72**, 650–654.
59 P. J. Hay and W. R. Wadt, *J. Chem. Phys.*, 1985, **82**, 270–283.
60 M. N. Glukhovtsev, A. Pross, M. P. McGrath and L. Radom, *J. Chem. Phys.*, 1995, **103**, 1878–1885.
61 A. L. L. East, G. M. Berner, A. D. Morcom and L. Mihichuk, *J. Chem. Theory Comput.*, 2008, **4**, 1274–1282.
62 S. S. Hepperle, Q. Li and A. L. L. East, *J. Phys. Chem. A*, 2005, **109**, 10975–10981.
63 C. Sosa, J. Andzelm, B. C. Elkin, E. Wimmer, K. D. Dobbs and D. A. Dixon, *J. Phys. Chem.*, 1992, **96**, 6630–6636.

64 N. Godbout, D. R. Salahub, J. Andzelm and E. Wimmer, *Can. J. Chem.*, 1992, **70**, 560–571.
65 F. H. Allen and I. J. Bruno, *Acta Crystallogr., Sect. B: Struct. Sci.*, 2010, **66**, 380–386.
66 H. Putz and K. Brandenburg, *Diamond - Crystal and Molecular Structure Visualization*, Germany, 2012.
67 W. Humphrey, A. Dalke and K. Schulten, *J. Mol. Graphics*, 1996, **14**, 33–38.
68 T. A. Keith, *AIMAll, TK Gristmill Software*, Overland Park KS, USA, 2012.
69 M. A. Spackman and J. J. McKinnon, *CrystEngComm*, 2002, **4**, 378–392.
70 M. A. Spackman and D. Jayatilaka, *CrystEngComm*, 2009, **11**, 19–32.
71 J. J. McKinnon, M. A. Spackman and A. S. Mitchell, *Acta Crystallogr., Sect. B: Struct. Sci.*, 2004, **60**, 627–668.
72 J. J. McKinnon, D. Jayatilaka and M. A. Spackman, *Chem. Commun.*, 2007, 3814–3816.
73 R. Berger, G. Resnati, P. Metrangolo, E. Weber and J. Hulliger, *Chem. Soc. Rev.*, 2011, **40**, 3496–3508.
74 P. A. Wood, J. J. McKinnon, S. Parsons, E. Pidcock and M. A. Spackman, *CrystEngComm*, 2008, **10**, 368–376.
75 M. O. Sinnokrot and C. D. Sherrill, *J. Phys. Chem. A*, 2006, **110**, 10656–10668.
76 M. I. Aroyo, A. Kirov, C. Capillas, J. M. Perez-Mato and H. Wondratschek, *Acta Crystallogr., Sect. A: Found. Crystallogr.*, 2006, **62**, 115–128.
77 A. M. Ilia, P.-M. Juan Manuel, C. Cesar, K. Eli, I. Svetoslav, M. Gotzon, K. Asen and W. Hans, *Z. Kristallogr.*, 2009, **221**, 15.
78 M. I. Aroyo, J. M. Perez-Mato, D. Orobengoa, E. Tasci, G. De La Flor and A. Kirov, *Bulg. Chem. Commun.*, 2011, **43**, 183–197.
79 C. Slebodnick, J. Zhao, R. Angel, B. E. Hanson, Y. Song, Z. Liu and R. J. Hemley, *Inorg. Chem.*, 2004, **43**, 5245–5252.
80 N. P. Funnell, A. Dawson, D. Francis, A. R. Lennie, W. G. Marshall, S. A. Moggach, J. E. Warren and S. Parsons, *CrystEngComm*, 2010, **12**, 2573–2583.
81 M. J. Cliffe and A. L. Goodwin, *J. Appl. Crystallogr.*, 2012, **45**, 1321–1329.

